Journal of Quantitative Spectroscopy & Radiative Transfer 149 (2014) 64–71

Contents lists available at ScienceDirect

Journal of Quantitative Spectroscopy & Radiative Transfer

journal homepage: www.elsevier.com/locate/jqsrt

Empirical determination of low J values of $^{13}CH_4$ transitions from jet cooled and 80 K cell spectra in the icosad region (7170–7367 cm^{-1})

O. Votava [a], M. Mašát [a,b], P. Pracna [a], D. Mondelain [c,d], S. Kassi [c,d], A.W. Liu [e], S.M. Hu [e], A. Campargue [c,d,*]

[a] J. Heyrovský Institute of Physical Chemistry, ASCR, Dolejškova 3, Prague 8, Czech Republic
[b] Institute of Organic Chemistry and Biochemistry, ASCR, Flemingovo nam. 2,16610 Prague 6, Czech Republic
[c] Université Grenoble Alpes, LIPhy, F-38000 Grenoble, France
[d] CNRS, LIPhy, F-38000 Grenoble, France
[e] Hefei National Laboratory for Physical Sciences at Microscale, Department of Chemical Physics, University of Science and Technology of China, Hefei 230026, China

ARTICLE INFO

Article history:
Received 13 June 2014
Received in revised form
10 July 2014
Accepted 13 July 2014
Available online 19 July 2014

Keywords:
$^{13}CH_4$
Methane
Cold spectra
CH_4
HITRAN

ABSTRACT

The absorption spectrum of $^{13}CH_4$ was recorded at two low temperatures in the icosad region near 1.38 μm, using direct absorption tunable diode lasers. Spectra were obtained using a cryogenic cell cooled at liquid nitrogen temperature (80 K) and a supersonic jet providing a 32 K rotational temperature in the 7173–7367 cm^{-1} and 7200–7354 cm^{-1} spectral intervals, respectively. Two lists of 4498 and 339 lines, including absolute line intensities, were constructed from the 80 K and jet spectra, respectively.

All the transitions observed in jet conditions were observed at 80 K. From the temperature variation of their line intensities, the corresponding lower state energy values were determined. The 339 derived empirical values of the J rotational quantum number are found close to integer values and are all smaller than 4, as a consequence of the efficient rotational cooling. Six $R(0)$ transitions have been identified providing key information on the origins of the vibrational bands which contribute to the very congested and not yet assigned $^{13}CH_4$ spectrum in the considered region of the icosad.

1. Introduction

This contribution is part of a vast project aiming to obtain from the experiment insights on the mostly not yet assigned near infrared absorption spectrum of methane. The present work is devoted to the study of the $^{13}CH_4$ spectrum in the icosad range near 1.38 μm. The icosad region corresponds to the $P=5$ polyad containing 20 vibrational levels and 134 sub-levels in strong rovibrational interaction ($P=2(\nu_1+\nu_3)+\nu_2+\nu_4$, is the polyad number where ν_i are the four normal mode vibrational quantum numbers). As a result of numerous resonance couplings, the absorption spectrum is highly congested at room temperature (20–30 transitions per cm^{-1}) with no regular rotational progressions and remains unassigned (except a few lines of the intense $\nu_2+2\nu_3$ band at 7496 cm^{-1}) [1,2]. This applies both to the main isotopologue, $^{12}CH_4$, and to the ^{13}C carbon substitute, $^{13}CH_4$, under consideration.

Up to recently, this lack of assignment and then of knowledge of the lower state energy value of the

* Corresponding author at: Université Grenoble Alpes, LIPhy, F-38000 Grenoble, France.
E-mail address: Alain.Campargue@ujf-grenoble.fr (A. Campargue).

http://dx.doi.org/10.1016/j.jqsrt.2014.07.012
0022-4073/

transitions was an important limitation for the analysis of the planetary atmospheres as the line intensities could not be extrapolated to the temperature conditions of the considered atmospheres. In these circumstances, an experimental approach was adopted consisting in deriving empirically the lower state energy, E_{emp}, from the variation of the intensities measured at two temperatures [3,4]. This "two-temperature method" was systematically applied to natural methane spectra recorded at 296 K and 80 K, between 5852 and 7919 cm^{-1}. In the strong absorbing tetradecad [5–7] and icosad [1,2] regions, Differential Absorption Spectroscopy (DAS) was used while in the 1.58 μm [8–13] and 1.28 μm [14] transparency windows, the spectra were recorded by high sensitivity CW-Cavity Ring Down Spectroscopy (CRDS). This approach has led to the construction of the Wang, Kassi, Leshchishina, Mondelain, Campargue (WKLMC) empirical line lists at 296 K and 80 K [6,15,16], including isotopologue identification ($^{12}CH_4$, $^{13}CH_4$ and CH_3D), position, intensity and empirical lower state energy. The 296 K list (55,262 lines) was adopted for the HITRAN2012 database in the region [17,18] while the 80 K list (73,225 lines) has been successfully applied for Titan [6,19–21], Saturn, Jupiter [22], Uranus [23] and Pluto [24]. Fig. 1 shows the overview of the WKLMC lists at 80 and 296 K [16].

During the construction of the WKLMC lists, the quality of the E_{emp} retrieval was found to degrade for low E_{emp} values. This is due to the smaller E_{emp} dependence of the ratio of the intensities at 80 and 296 K. For instance, to discriminate transitions from $J=0$ and $J=1$ lower state energies ($E_{emp}=0$ and 10.48 cm^{-1}, respectively), the corresponding line intensity ratios have to be determined with an accuracy better than 7% [6], which is not easy considering the frequent line overlappings.

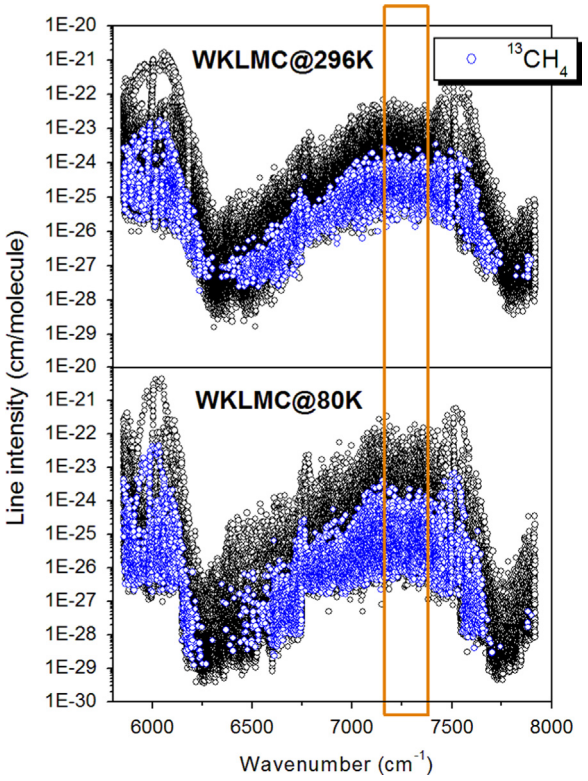

Fig. 1. Overview comparison of the WKLMC lists for natural methane at 80 and 296 K [6]. Lines due to $^{13}CH_4$ in natural abundance are highlighted. The spectral interval of the spectra of $^{13}CH_4$ at 80 K analyzed in this work is indicated.

In order to determine more accurately the low E_{emp} values, the 80 K line intensities can be advantageously combined to jet intensity data instead of room temperature intensities [25]. Very recently, by applying the two temperature method to jet spectra at 28 K and cell spectra at 80 K, 654 E_{emp} values of $^{12}CH_4$ transitions were accurately determined between 7050 and 7350 cm^{-1} [26]. The better accuracy of the retrieved E_{emp} values, illustrated by the histograms of the corresponding J_{emp} values (see Fig. 7 of Ref. [26]), results from a better contrast of the low J intensity ratios and, more importantly, from the total absence of line overlapping in the jet spectrum which makes the line intensity retrieval more accurate.

In the present work, we apply the same approach to the $^{13}CH_4$ isotopologue: the 80 K spectrum was recorded between 7173 and 7367 cm^{-1} while the jet spectrum covers the 7200–7354 cm^{-1} interval.

In the tetradecad region (5850–6150 cm^{-1}), the HITRAN2012 line list of $^{13}CH_4$ reproduce the positions, intensities and E_{emp} values obtained from spectra highly enriched in $^{13}CH_4$ [27]. A similar study with pure $^{13}CH_4$ sample is not yet available in the icosad and, to the best of our knowledge, the information available for $^{13}CH_4$ in the icosad is limited to the data included in the WKLMC lists [16] which were obtained from natural methane (see Fig. 1) and are reproduced in HITRAN2012. In the 7173–7367 cm^{-1} interval, the WKLMC lists at 296 K and 80 K include 160 and 696 $^{13}CH_4$ lines (excluding $^{13}CH_4$ lines blended by other isotopologues), respectively, but only 63 transitions were found in common in the 296 K and 80 K data sets and used for E_{emp} derivation by the 2T-method [16]. This is a consequence of the low natural abundance of $^{13}CH_4$ (about 1.1%), $^{13}CH_4$ lines being weak and frequently obscured by $^{12}CH_4$ lines, in particular at room temperature.

The aim of this present study is then a better characterization of the low J transitions of $^{13}CH_4$ in the 7173–7367 cm^{-1} interval, by using highly enriched $^{13}CH_4$ spectra recorded in a cryogenic cell cooled at liquid nitrogen temperature (80 K) and a supersonic jet providing a 32 K rotational temperature.

The rest of this report is organized as follows: The experimental set ups used for the cell and jet recordings are described in Section 2. The line list constructions and the determination of the lower state energy values are presented in Section 3. The obtained results are discussed in Section 4.

2. Experiment

The 80 K and jet spectra were recorded by Direct Absorption Spectroscopy (DAS) in Grenoble and in Prague, respectively. Both the liquid-nitrogen cooled cell experiment and the supersonic pulsed-jet experiment have been described in detail previously and only an outline is presented hereafter.

2.1. Cell spectra at 80 K

The experimental set up used for the bulk recordings at 80 K is the same as that used for methane in "natural" isotopic abundance. The DAS spectrometer and the design of the cryogenic cell cooled at liquid nitrogen temperature have been described in detail in Refs. [1,4,28]. The 7173–7367 cm^{-1} interval was covered thanks to seven fiber-connected Distributed Feed-Back (DFB) diode lasers (10–20 mW from NEL). The main part of the laser power is sent into a 1.42 m long cryogenic absorption cell cooled with liquid nitrogen, where the gas is cooled down to a temperature of 80 ± 2 K [4]. An absorption path length of 284 cm is achieved with one round trip in this cell. For each laser diode, the recorded transmission spectrum is the ratio of a transmitted spectrum over a reference spectrum acquired simultaneously over the whole laser tuning range ($\sim$35 cm^{-1}). This tuning range is obtained from the superimposition of a fast periodic current ramp and a slow temperature ramp from -10 to 60 °C [28]. Each final spectrum contains about 10^5 spectral points separated by a 10 MHz interval, well below the Doppler width of methane lines at 80 K (about 150 MHz HWHM).

The methane sample enriched in ^{13}C (>99%) was purchased from Isotec, Inc. During the recordings, the pressure (6.0 Torr at 80 K) was measured by a capacitance gauge (MKS Baratron type 626B, 10 Torr range, 0.25% accuracy). The noise equivalent absorption coefficient (NEA) evaluated as the *rms* deviation of the baseline fluctuation, is on the order of $\alpha_{min} \approx 5 \times 10^{-8}$ cm^{-1}.

A first wavenumber calibration of each spectrum was obtained from a wavelength meter (621A, Bristol Instruments). To increase the wavenumber accuracy an additional absolute calibration is needed. It was performed by statistically matching the recorded line positions with accurate positions obtained from a room temperature spectrum of $^{13}CH_4$ recorded at USTC-Hefei by Fourier Transform Spectroscopy (P=4 Torr, l=15 m, unapodized resolution of 0.015 cm^{-1}). This FTS spectrum was itself calibrated against line positions of H_2O (present as an impurity) from the HITRAN database [18].

For each complete laser diode spectrum, the *rms* values of the difference between the DAS and reference line positions are generally between 5×10^{-4} and 1×10^{-3} cm^{-1}. The average uncertainty of the absolute values of the centers of the well isolated lines is then believed to be less than 1×10^{-3} cm^{-1}.

2.2. Jet spectra

The Prague supersonic jet near-IR spectrometer has been described previously [25,26], and thus only specific changes relevant to the current project are discussed in some detail. The experimental setup consists of a pulsed slit-jet supersonic source of cold molecules coupled with a high-resolution cw diode laser direct absorption spectrometer. It is tunable between 7070 and 7300 cm^{-1} with an output power of about 3 mW. The supersonic beam through 40 mm × 0.1 mm slit nozzle is pulsed using custom designed fast solenoid valve. Typically 1 ms long gas pulses at repetition rate of 3 Hz are used. This source provides intense beam of cold molecules (temperatures down to $\sim$20 K have been achieved for methane expanded in Ar [25]). In the present work, we used a 1:1 mixture of methane and argon at total stagnation pressure of 300 Torr. The temperature was determined to be 32(2) K from the Doppler broadening of a series of measured spectral lines.

One of the intrinsic features of the free-jet supersonic expansion experiments is the high sample consumption compared to static or slow-flowing spectroscopic cells. With the present experimental conditions the average methane flow rate is $\sim$20 sccm/min. This represents certain limitation in case of expensive samples such as the isotopically enriched species of methane in this particular case. All the jet data presented in this paper have been measured using 100 standard liters of $^{13}CH_4$ gas (purity >99%). This allows for approximately 80 h of continuous experiment running and corresponds to 400 cm^{-1} of single mode spectral scans at typical scan rate of 5 cm^{-1}/h, which are typical scanning rates for the diode laser spectrometer. Since reliable line list is typically constructed from minimum of two complete spectral scans, the available sample is indeed close to the minimum amount required for covering the 7200–7354 cm^{-1} interval.

To minimize the $^{13}CH_4$ consumption, the gas inlet system was modified to allow for rapid switching between the natural methane and $^{13}CH_4$ samples, while maintaining the expansion conditions identical for both species: a three-way valve with flow-controlling needle valve on the output branch was placed as close as possible to the pulsed nozzle inlet. Natural methane and the $^{13}CH_4$ sample tanks were connected *via* pressure regulators set at identical pressures to the two input branches of the three-way valve. The dead volume between the three way valve and the nozzle was estimated to be less than 10 cm^3, so the purge time after switching from one branch to the other was on the order of 1 min. This is verified by measuring the disappearance rate of selected $^{12}CH_4$ absorption line after switching to the $^{13}CH_4$ sample. Thus all the experiment alignment and signal optimization were performed using natural methane. In addition, selected $^{12}CH_4$ spectral transition was needed for both frequency and intensity calibration, as described in some details below.

The laser spectrometer setup is identical to that described previously [25,26]. Extended cavity diode laser in Littman configuration can be tuned from 7180 to 7360 cm^{-1} using a single laser diode. Coarse tuning is achieved using a DC motor driven micrometric screw, while fine single-mode scans (up to 7 cm^{-1}/scan) are performed by applying voltage to a piezo transducer. Both the coarse and fine tuning/scanning are done automatically under computer control so that a sequence of partially overlapped single mode scans is recorded. Frequency steps separated by 7×10^{-4} cm^{-1} were chosen providing about 10 data points over the full-width-at-half-maximum (FWHM) of the Doppler broadened methane spectral lines at 32 K. At each gas pulse a single absorption measurement is performed, taking one measurement per laser frequency step.

Direct absorption measurements are performed with a dual-beam differential arrangement using a custom auto-balanced detector. The signal laser beam is double passed through the supersonic jet for a total absorption path length of about 8 cm. Intensity noise of this direct absorption arrangement is 2×10^{-5}, dominated by the residual amplitude noise of the laser due to imperfect noise subtraction on the auto-balanced dual beam detector. The NEA of the jet experiment is thus $\alpha_{min}\approx2.5\times10^{-6}\,\mathrm{cm}^{-1}$. The weakest spectral lines in the jet spectra observed at on-peak $S/N\sim2$ have integrated line intensity near 1.75×10^{-24} cm/molecule, while the strongest line in the investigated spectral range has an intensity of 7.5×10^{-22} cm/molecule.

Relative frequency calibration of the spectral scans was done using a combination of Michelson wavemeter and temperature stabilized Fabry-Perot etalon with long term frequency drift estimated at $\sim1\times10^{-4}\,\mathrm{cm}^{-1}$ over 24 h period. Absolute calibration was achieved by referencing all spectra to the position of the $^{12}CH_4$ calibration line at 7313.8078 cm^{-1} [16]. Utilizing the capability for rapid switching between the natural methane and ^{13}C methane as described above the reference line was scanned before and after each batch of ^{13}C spectral scans (typically 4–8 consecutive spectral scans). Frequency calibration was further verified by agreement with the cold cell measurements: Standard deviation of differences between the cell spectra and the jet spectra for all the matched lines in two-temperature analysis is $4.7\times10^{-4}\,\mathrm{cm}^{-1}$. We have observed that the integrated line intensity of the reference line measured before and after each data batch does not differ by more than 5%, thus it is assumed that the methane number density remains constant to this precision throughout the data batch.

The considerable change of the appearance of the spectra induced by cooling down from room to jet temperature is illustrated in Fig. 2.

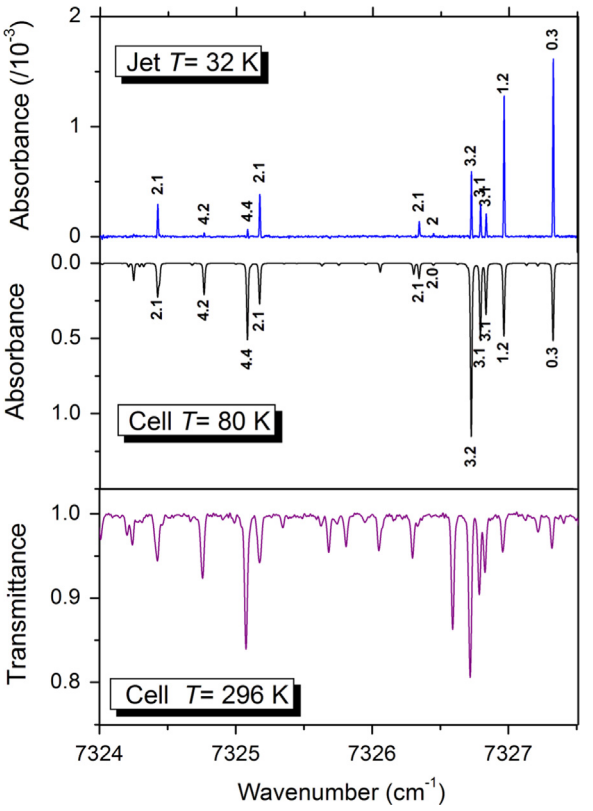

Fig. 2. Comparison of the $^{13}CH_4$ spectrum recorded by Differential Absorption Spectroscopy near 7325 cm^{-1}, in a supersonic jet with rotational temperature of 32 K (top) and in a cryogenic cell at 80 K (middle) to a FTS spectrum at room temperature (bottom). The experimental conditions were (P=6.0 Torr, l=2.84 m) and (P=4.0 Torr, l=15 m) for the cell spectra at 80 K and 296 K, respectively. On the two upper panels, the derived empirical values of the lower state rotational quantum number are given (see Section 3).

2.3. Construction of the line lists

The line intensity, S_{ν_0} (cm/molecule), of a rovibrational transition centered at ν_0, is related to the integrated line absorbance, expressed as

$$\int_{line}\alpha_\nu l\,d\nu=\int_{line}\ln\left[\frac{I_0(\nu)}{I(\nu)}\right]d\nu=S_{\nu_0}(T)Nl \qquad (1)$$

where ν is the wavenumber in cm^{-1}, $I_0(\nu)/I(\nu)$ is the ratio of the incident intensity to the transmitted intensity, l is the absorption pathlength, $\alpha(\nu)$ is the absorption coefficient in cm^{-1}, and N is the absorber concentration in molecule/cm^3.

In the case of the bulk spectra at 80 K, absolute intensity values are readily obtained from the integrated line absorbance as the absorption pathlength is known (l=284 cm) and the molecular density is calculated from the measured pressure value: $P=Nk_BT$. This is not the case for the jet spectra where a scaling of the derived integrated line absorbances is necessary to obtain absolute intensity values in the jet conditions.

An interactive multi-line fitting program (http://fityk.nieto.pl/) was used to least square fit the spectra to derive the integrated line absorbances. In the case of the jet spectra, a Gaussian line profile corresponding to the Doppler broadening was used. The local baseline, line center, integrated absorbance and HWHM of the Gaussian function were fitted. An average expansion temperature of 32(2) K was deduced from the derived Gaussian widths.

At 80 K, the pressure self line broadening – on the order 0.20 cm^{-1}/atm [29] – contributes significantly to the observed line profile: $1.6\times10^{-3}\,\mathrm{cm}^{-1}$ (HWHM) at 6 Torr to be compared to the 80 K Doppler broadening of $5.7\times10^{-3}\,\mathrm{cm}^{-1}$ (HWHM). Consequently, a Voigt function of the wavenumber was adopted as line profile for the 80 K spectra. The HWHM of the Gaussian component was fixed to its theoretical value. The local baseline (assumed to be a quadratic function of the wavenumber) and the three parameters of each Voigt profile (line center, integrated absorbance, HWHM of the Lorentzian component) were fitted. In the case of blended lines or lines with low signal to noise ratios, the Lorentzian HWHM was also constrained to the average value obtained from nearby isolated lines.

By gathering the line lists corresponding to the different DFB laser diodes, a list of 4498 lines (Fig. 3) was obtained from the 80 K spectra (to be compared to 696

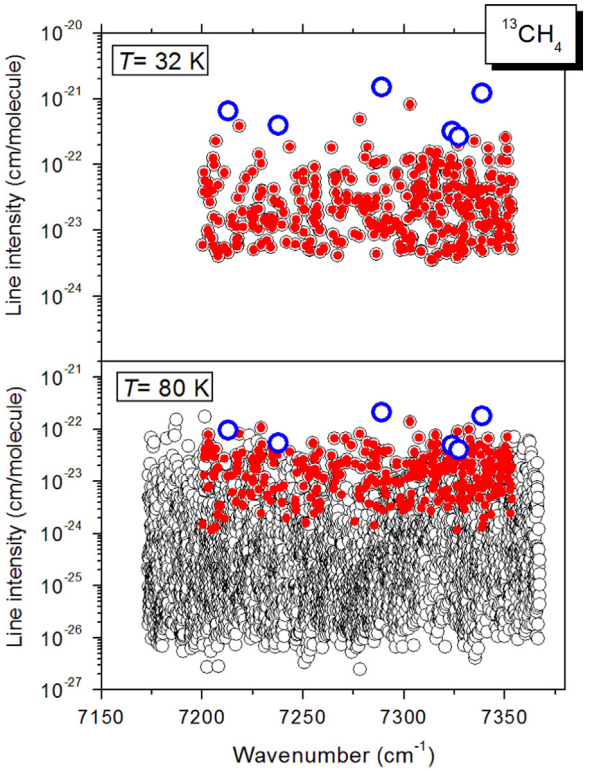

Fig. 3. Overview of the jet and cell line lists of $^{13}CH_4$ in the 7173–7367 cm^{-1} and 7200–7354 cm^{-1} spectral interval, respectively. The 339 transitions for which the E_{emp} values were derived by the 2T-method, are highlighted in red. The blue open circles correspond to the six transitions identified as $R(0)$. (For interpretation of the references to color in this figure legend, the reader is referred to the web version of this article.)

$^{13}CH_4$ lines in the WKLMC@80K list in the same 7173–7367 cm^{-1} region). The weakest lines have intensity on the order of 5×10^{-27} cm/molecule at 80 K. As expected, the use of a pure $^{13}CH_4$ sample allowed lowering by two orders of magnitude the intensity threshold of $^{13}CH_4$ in the WKLMC@80K list.

As mentioned above, a calibration procedure must be performed to convert the jet integrated absorbances to absolute intensity values in jet temperature conditions. The $^{12}CH_4$ line at 7313.8078 cm^{-1} was selected as reference line as it is one of the strongest $^{12}CH_4$ transitions in the region [16]. It was also identified as a $R(0)$ transition in our $^{12}CH_4$ study [26]. The reference line spectrum was recorded at the beginning and the end of each $^{13}CH_4$ data batch. Using the absolute intensity value at 28 K of the $^{12}CH_4$ reference line (8.26×10^{-22} cm/molecule [26]), the integrated line absorbances were converted to absolute line intensities. Overall, the jet dataset (upper panel of Fig. 3) includes 339 lines between 7200 and 7354 cm^{-1}, with intensity ranging between 1.7×10^{-24} and 7.5×10^{-22} cm/molecule.

3. Determination of the lower state energy

The 339 lines of the jet list were unambiguously matched with corresponding transitions in the 80 K line list. The associated lines are highlighted on the overview of

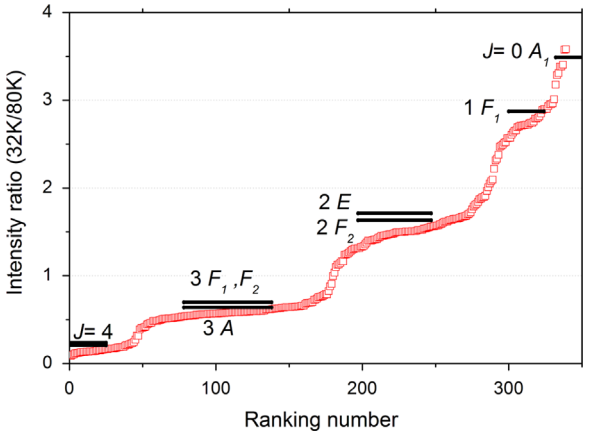

Fig. 4. Ratios of the line intensities in the jet (32 K) and cooled cell (80 K) spectra of $^{13}CH_4$ in the 7200–7354 cm^{-1} spectral interval. The ratios are ranked in increasing order. Horizontal lines correspond to the theoretical values of the intensity ratios calculated in absence of nuclear spin conversion during the expansion [25]. The corresponding J quantum number and rotational symmetry are indicated.

the line lists displayed in Fig. 3. Their intensity ratios which are plotted in increasing order in Fig. 4, were used to derive the E_{emp} energy values by using the 2T-method.

In general, for a given transition measured at two temperatures (T_0 and T_1), the lower state energy value is obtained from

$$\ln\left(\frac{S_{v_0}(T_1)Q(T_1)}{S_{v_0}(T_0)Q(T_0)}\right)=-E_{emp}\left[\frac{1}{kT_0}-\frac{1}{kT_1}\right] \quad (2)$$

where $S(T)$ and $Q(T)$ are the line intensities and partition function, respectively.

Using the approximate ground state term value $E=B_0J(J+1)$, the corresponding empirical rotational quantum number, J, can be computed from $J_{emp}=\sqrt{(1/4)+(E/B_0)}-(1/2)$ where $B_0=5.214$ cm^{-1} is the $^{13}CH_4$ ground state rotational constant.

At thermodynamic equilibrium like in our cryogenic cell at 80 K, the methane partition function is accurately known from calculations, $Q(80\text{ K})=83.7$ [18]. In jet conditions, the situation is made more complicated by the fact that thermodynamic equilibrium is not reached. Several studies [25,30–36] have showed that the nuclear spin conversion is inefficient in the expansion and the spin isomers relative populations existing at thermodynamic equilibrium are unchanged during the expansion. Since methane has three nuclear spin isomers with quantum number $I=2$ (meta), $I=1$ (ortho), and $I=0$ (para), the relative populations within the spin isomers are 5:9:2 at equilibrium [25]. During the expansion, these values do not change and thermodynamic equilibrium is established separately within each nuclear spin isomer, but not between them. In particular, at zero temperature limit, all the molecules will not accumulate in the $J=0$ level but will be distributed between the lowest meta ($J=0$ A_1), ortho ($J=1$ F_1) and para ($J=2$ E) levels in the 5:9:2 proportion. We have included in Fig. 4, the intensity ratios for J values up to 4, calculated in Ref. [25] taking into account the nuclear-spin conservation. The good

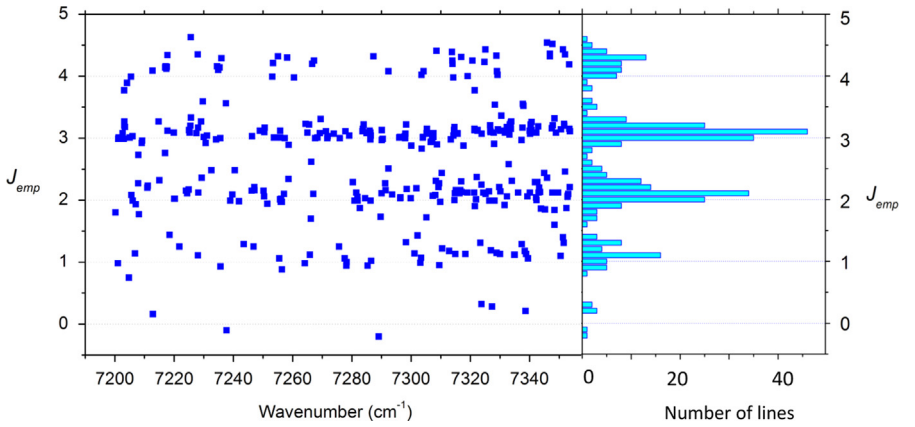

Fig. 5. *Left hand panel*: Empirical lower J values *versus* the line positions in the 7200–7354 cm^{-1} spectral interval of the icosad of $^{13}CH_4$. *Right hand panel*: Corresponding histogram of the empirical lower J values.

Table 1
Wavenumbers and line intensities at 32 K and 80 K of the $^{13}CH_4$ transitions identified as $R(0)$ transitions from the variation of their line intensities. Intensity values correspond to pure $^{13}CH_4$.

Jet (T=32 K)		Cell (T=80 K)		*Int. ratio*	E_{emp} (cm^{-1})	J_{emp}
Center (cm^{-1})	*Intensity* (*cm/molecule*)	*Center* (cm^{-1})	*Intensity* (*cm/molecule*)			
7212.815	3.23×10^{-22}	7212.815	9.51×10^{-23}	3.40	0.9	0.16
7237.713	1.97×10^{-22}	7237.714	5.52×10^{-23}	3.57	−0.82	−0.19
7289.109	7.52×10^{-22}	7289.108	2.10×10^{-22}	3.58	−0.92	−0.23
7323.754	1.60×10^{-22}	7323.754	4.87×10^{-23}	3.29	2.2	0.32
7327.319	1.33×10^{-22}	7327.318	4.03×10^{-23}	3.31	1.9	0.28
7338.623	5.99×10^{-22}	7338.623	1.78×10^{-22}	3.37	1.3	0.26

coincidence between the measured and predicted intensity ratios leaves no doubt on the J identification for most of the lines.

As the partition function in jet depends not only on the temperature, but also on the nuclear spin isomer, three partition functions are at disposal for the derivation of the E_{emp} value by the 2T-method (Eq. (2)). Their values at 32 K have been evaluated in Ref. [25]: $Q_{meta}(32\text{ K})=23.94$, $Q_{ortho}(32\text{ K})=21.92$ and $Q_{para}(32\text{ K})=20.91$ (the thermodynamic equilibrium value is $Q_{eq}(32\text{ K})=22.4$). The choice of the partition function is unambiguous in the case of the J=0 and J=1 levels, which are associated to a single isomer species (ortho and meta, respectively). In the case of the J=2 and J=3 levels, each one associated to two isomer species (ortho–para and meta–ortho, respectively – see Fig. 4), the average value of the two relevant partition functions was used, while the equilibrium value was adopted for the J=4 levels. The procedure consisted then in two steps: first an approximate J value was derived using $Q_{eq}(32\text{ K})$, then, according to the nearest integer value, a refined J value was determined using the most appropriate value of the partition function. Note that the good choice of the partition function is crucial to discriminate the J=0 and 1 levels which have close line intensity temperature dependence (difference of about 20% on the intensity ratios at 80 and 32 K [25]) while it is less important for the J=2–4 levels which show a much larger contrast (see Fig. 4). As a consequence, the approximation used for the partition function of the J=2–4 levels is fully justified.

Let us recall that the intensity ratio can be potentially used to distinguish the nuclear-spin components for a given J value [25] but the contrast is small and in fact insufficient compared to our experimental error bars. If we consider the most favorable case of the J=2, E and F_2 components, an experimental uncertainty on the intensity ratios better than 5% is required to discriminate the two components.

The full jet and cell line lists including the obtained E_{emp} and J_{emp} values are provided as Supplementary material. As an example, the J_{emp} values have been indicated in the spectra displayed in Fig. 2. The obtained J_{emp} values are displayed in Fig. 5 *versus* the line positions. The corresponding histogram included in the same figure illustrates the propensity of J_{emp} to be close to integer values. Only for six transitions listed in Table 1, a J_{emp} value close to 0 is obtained. They are among the strongest transitions of the 7200–7354 cm^{-1} region both in the jet and cell spectra (see Fig. 3 where they have been highlighted).

4. Concluding remarks

Fig. 6 presents an overview comparison of our $^{13}CH_4$ line list at 80 K to that extracted from the WKLMC@80K list of natural methane (line intensities have been

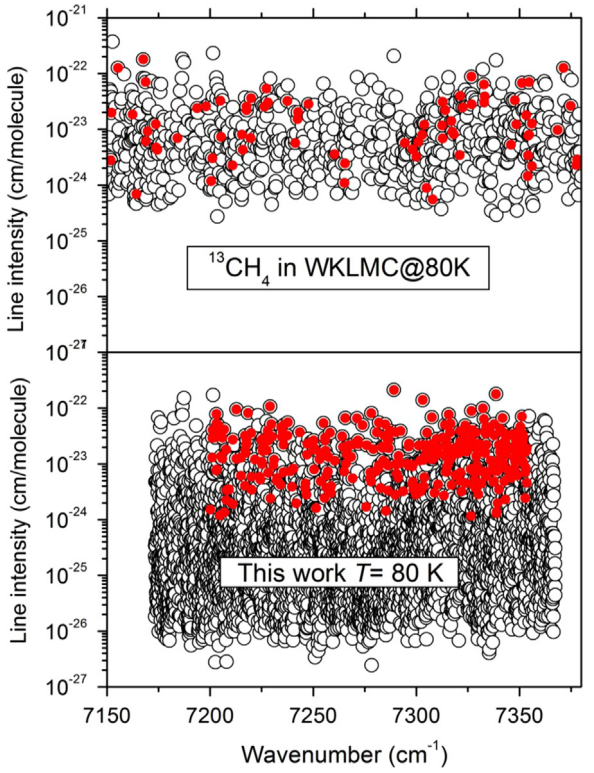

Fig. 6. Overview comparison of the $^{13}CH_4$ line lists at 80 K obtained in this work (lower panel) and extracted from the WKLMC@80K list of natural methane (line intensities have been corrected from the $^{13}CH_4$ abundance) [16]. The transitions with derived E_{emp} values have been highlighted on the two panels.

corrected from the $^{13}CH_4$ abundance) [16]. The transitions with derived E_{emp} values have been highlighted. Even for the strongest lines, many E_{emp} values are missing in the WKLMC@80K list because $^{13}CH_4$ lines are weak and frequently obscured by $^{12}CH_4$ lines in the methane spectrum, in particular at room temperature. As a result, many $^{13}CH_4$ lines observed at 80 K were not observed at 296 K, preventing the application of the 2*T*-method. The presently obtained line list at 80 K with derived E_{emp} values may be used to improve the $^{13}CH_4$ parameters in the WKLMC list at 80 K and add E_{emp} values in the WKLMC list at 296 K but a difficulty will be to treat properly the intensities of the lines of the WKLMC lists involving the contribution of two isotopologues [6].

Similarly to our previous study of $^{12}CH_4$ in the same region [26], we failed in associating $P(1)$, $Q(1)$, $R(1)$ lines to the lines identified as $R(0)$ (Table 1). This confirms the strength of the numerous resonance interactions existing in the region and underlines the significance of the obtained results for future assignment of the spectrum in an energy region particularly difficult to model.

Up to now, the only states of the $^{12}CH_4$ icosad which have been modeled using effective Hamiltonians are those located at the low and high energy limits of the polyad: namely the $5\nu_4$ and $\nu_2+4\nu_4$ band systems near 6400 cm^{-1} [13] and to a lesser extent, the $\nu_2+2\nu_3$ band at 7510 cm^{-1} [35] (which is shifted to 7496 cm^{-1} in $^{13}CH_4$). Being located near the borders of the icosad, these levels are less affected by interactions while those located in the presently spectral interval are considerably more perturbed. Indeed, at present, the icosad constitutes the high energy limit for the spectroscopic empirical models which were applied to the lower polyads up to the tetradecad [37]. In the icosad, the number of interacting states (20 vibrational levels and 134 sub-levels) leads to a prohibitive number of interaction parameters to be fitted. A new approach has recently be proposed, consisting in deriving the resonance coupling parameters of the effective polyad Hamiltonians *via* high-order contact transformations from a high accuracy *ab initio* potential energy (PES) [38]. Alternatively, global variational methods based on accurate *ab initio* potential energy and dipole moment surfaces appear to be the most promising to further assign the methane spectrum at high energy [39]. Even if this approach cannot achieve the experimental accuracy, it has been successfully applied up to the tetradecad region of $^{12}CH_4$ [39] and has provided vibrational assignment [40] for all but one $R(0)$ icosad transitions of $^{12}CH_4$ identified in Ref. [26]. Very convincing is the fact that the only $R(0)$ line which could not be assigned, at 7152.7215 cm^{-1}, belongs in fact to $^{13}CH_4$ in natural abundance in the methane sample of Ref. [26].

The important set of 339 empirical low J values of $^{13}CH_4$ determined in the present study provides then valuable experimental information for constraining, validating or refining theoretical models. Let us note that an interesting approach already applied in the tetradecad consists in transferring to $^{13}CH_4$ the assignments obtained for $^{12}CH_4$, by using the isotopic shift values which can be accurately computed from an *ab initio* PES [41,42]. The isotopic substitution shift being calculated with a higher (<1 cm^{-1}) absolute accuracy than the energy levels, a one-to-one correspondence can be achieved between $^{13}CH_4$ and $^{12}CH_4$ lines, at least for the strongest lines.

Acknowledgments

This work was performed in the frame of the Labex-OSUG@2020 (ANR10 LABX56). O.V. would like to acknowledge support from the Grant Agency of the Czech Republic, Project number 13-11635S.

Appendix A. Supplementary material

Supplementary data associated with this article can be found in the online version at http://dx.doi.org/10.1016/j.jqsrt.2014.07.012.

References

[1] Campargue A, Wang L, Kassi S, Mašát M, Votava O. Temperature dependence of the absorption spectrum of CH_4 by high resolution spectroscopy at 81 K: (II) the Icosad region (1.49–1.30 μm). J Quant Spectrosc Radiat Transf 2010;111:1141–51.

[2] Wang L, Mondelain D, Kassi S, Campargue A. The absorption spectrum of methane at 80 and 294 K in the Icosad (6717–7589 cm^{-1}): improved empirical line lists, isotopologue identification and temperature dependence. J Quant Spectrosc Radiat Transf 2011;113:47–57.

[3] Kassi S, Gao B, Romanini D, Campargue A. The near infrared (1.30–1.70 μm) absorption spectrum of methane down to 77 K. Phys Chem Chem Phys 2008;10:4410–9.
[4] Gao B, Kassi S, Campargue A. Empirical low energy values for methane transitions in the 5852–6181 cm^{-1} region by absorption spectroscopy at 81 K. J Mol Spectrosc 2009;253:55–63.
[5] Wang L, Kassi S, Campargue A. Temperature dependence of the absorption spectrum of CH_4 in the region of the $2n_3$ band at 1.66 μm by absorption spectroscopy at 81 K. J Quant Spectrosc Radiat Transf 2010;111:1130–40.
[6] Campargue A, Wang L, Kassi S, Mondelain D, Bézard B, Lellouch E, et al. An empirical line list for methane in the 1.26–1.71 μm region for planetary investigations ($T\sim$80–300 K). Application to Titan. Icarus 2012;219:110–28.
[7] Campargue A, Leshchishina O, Wang L, Mondelain D, Kassi S, Coustenis A. An improved empirical line list for methane in the region of the $2\nu_3$ band at 1.66 μm. J Quant Spectrosc Radiat Transf 2013;118:49–59.
[8] Liu AW, Kassi S, Campargue A. High sensitivity CW-cavity ring down spectroscopy of CH_4 in the 1.55 μm transparency window. Chem Phys Lett 2007;447:16–20.
[9] Kassi S, Romanini D, Campargue A. Mode by Mode CW-CRDS at 80 K: application to the 1.58 μm transparency window of CH_4. Chem Phys Lett 2009;477:17–21.
[10] Campargue A, Wang L, Liu AW, Hu SM, Kassi S. Empirical line parameters of methane in the 1.63–1.48 μm transparency window by high sensitivity Cavity Ring Down Spectroscopy. Chem Phys 2010;373:203–10.
[11] Wang L, Kassi S, Liu AW, Hu SM, Campargue A. High sensitivity absorption spectroscopy of methane at 80 K in the 1.58 μm transparency window: temperature dependence and importance of the CH_3D contribution. J Mol Spectrosc 2010;261:41–52.
[12] Wang L, Kassi S, Liu AW, Hu SM, Campargue A. The 1.58 μm transparency window of methane (6165–6750 cm^{-1}): empirical line list and temperature dependence between 80 K and 296 K. J Quant Spectrosc Radiat Transf 2011;112:937–51.
[13] Nikitin AV, Thomas X, Régalia L, Daumont L, Von der Heyden P, Tyuterev VIG, et al. Assignment of the $5\nu_4$ and $\nu_2+4\nu_4$ band systems of $^{12}CH_4$ in the 6287–6550 cm^{-1} region. J Quant Spectrosc Radiat Transf 2011;112:28–40.
[14] Mondelain D, Kassi S, Wang L, Campargue A. The 1.28 μm transparency window of methane (6165–6750 cm^{-1}): empirical line list and temperature dependence between 80 K and 296 K. Phys Chem Chem Phys 2011;17:7985–96.
[15] Campargue A, Leshchishina O, Wang L, Mondelain D, Kassi S, Nikitin AV. Refinements of the WKMC empirical line lists (5852–7919 cm^{-1}) for methane between 80 K and 296 K. J Quant Spectrosc Radiat Transf 2012;113:1855–73.
[16] Campargue A, Leshchishina O, Wang L, Mondelain D, Kassi S. The WKLMC empirical line lists (5852–7919 cm^{-1}) for methane between 80 K and 296 K: "final" lists for atmospheric and planetary applications. J Mol Spectrosc 2013;291:16–22.
[17] Brown LR, Sung K, Benner DC, Devi VM, Boudon V, Gabard T, et al. Methane line parameters in the HITRAN2012 database. J Quant Spectrosc Radiat Transf 2013;130:201–19.
[18] Rothman LS, Gordon IE, Babikov YL, Barbe A, Benner DC, Bernath PF, et al. The HITRAN2012 molecular spectroscopic database. J Quant Spectrosc Radiat Transf 2013;130:4–50.
[19] de Bergh C, Courtin R, Bézard B, Coustenis C, Lellouch E, Hirtzig M, et al. Applications of a new set of methane line parameters to the modeling of Titan's spectrum in the 1.58-micron window. Planet Space Sci 2012;61:85–98.
[20] Hirtzig M, Bézard B, Lellouch E, Coustenis A, de Bergh C, Drossart P, et al. Titan's surface and atmosphere from Cassini/VIMS data with updated methane opacity. Icarus 2013;226:470–86.
[21] Bailey J, Ahlsved L, Meadows VS. The near-IR spectrum of Titan modelled with an improved methane line list. Icarus 2011;213:218–32.
[22] Sromovsky LA, Fry PM, Boudon V, Campargue A, Nikitin AV. Comparison of line-by-line and band models of near-IR methaneabsorption applied to outer planet atmospheres. Icarus 2012;218:1–23.
[23] Irwin PGJ, de Bergh C, Courtin R, Bézard B, Teanby NA, Davis GR, et al. The application of new methane line absorption data to Gemini-N/NIFS and KPNO/FTS observations of Uranus' near-infrared spectrum. Icarus 2012;220:369–82.
[24] Lellouch E, Sicardy B, de Bergh C, Käufl HU, Kassi S, Campargue A. Pluto's lower atmosphere structure and methane abundance from high-resolution spectroscopy and stellar occultations. Astron Astrophys 2009;495:17–21.
[25] Votava O, Mašát M, Pracna P, Kassi S, Campargue A. Accurate determination of low state rotational quantum numbers ($J<4$) from planar-jet and liquid nitrogen cell absorption spectra of methane near 1.4 μm. Phys Chem Chem Phys 2010;12:3145–55.
[26] Mašát M, Pracna P, Mondelain D, Kassi S, Campargue A, Votava O. Spectroscopy of jet-cooled methane in the lower icosad region: empirical assignments of low-J spectral lines from two-temperature analysis. J Mol Spectrosc 2013;291:9–15.
[27] Lyulin OM, Kassi S, Sung K, Brown LR, Campargue A. Determination of the low energy values of $^{13}CH_4$ transitions in the $2\nu_3$ region near 1.66 μm from absorption spectra at 296 and 81 K. J Mol Spectrosc 2010;261:91–100.
[28] Lu Y, Mondelain D, Kassi S, Campargue A. The CH_3D absorption spectrum in the 1.58 μm transparency window of methane: empirical line lists and temperature dependence between 80 K and 296 K. J Quant Spectrosc Radiat Transf 2011;112:2683–97.
[29] Menard-Bourcin F, Menard J, Boursier C. Temperature dependence of rotational relaxation of methane in the $2\nu_3$ vibrational state by self- and nitrogen-collisions and comparison with line broadening measurements. J Mol Spectrosc 2007;242:55–63.
[30] Boraas K, De Boer DF, Lin Z, Reilly JP. The Stark effect in methane's $3\nu_1+\nu_3$ vibrational overtone band. J Chem Phys 1993;99:1429–32.
[31] Hippler M, Quack M. CW-cavity ring-down infrared absorption spectroscopy in pulsed supersonic jets: nitrous oxide and methane. Chem Phys Lett 1999;314:273–81.
[32] Amrein A, Quack M, Schmitt U. High resolution interferometric Fourier transform infrared absorption spectroscopy in supersonic free jet expansions: carbon monoxide, nitric oxide, methane, ethyne, propyne, and trifluoromethane. J Phys Chem 1988;92:5455–66.
[33] Hippler M, Quack M. High-resolution Fourier transform infrared and CW-diode laser cavity ringdown spectroscopy of the $\nu_2+2\nu_3$ band of CH_4 near 7510 cm^{-1} in slit jet expansions and at room temperature. J Chem Phys 2002;116:6045–55.
[34] Campargue A, Chenevier M, Stoeckel F. Intracavity-laser-absorption spectroscopy of the visible overtone transition of methane in a supersonically cooled jet. Chem Phys Lett 1991;183:153–7.
[35] Manca Tanner C, Quack M. Reinvestigation of the $\nu_2+2\nu_3$ subband in the overtone icosad of $^{12}CH_4$ using cavity ring-down (CRD) spectroscopy of a supersonic jet expansion. Mol Phys 2012;113:2111–35.
[36] Campargue A, Permogorov D, Jost R. Intracavity absorption spectroscopy of the third stretching overtone transition of jet cooled methane. J Chem Phys 1995;102:5910–6.
[37] Nikitin AV, Boudon V, Wenger Ch, Albert S, Brown LR, Bauerecker S, et al. High resolution spectroscopy and the first global analysis of the tetradecad region of methane $^{12}CH_4$. Phys Chem Chem Phys 2013;15:10071–93.
[38] Tyuterev VLG, Tashkun SA, Rey M, Kochanov R, Nikitin A, Delahaye T. Accurate spectroscopic models for methane polyads derived from a potential energy surface using high-order contact transformations. J Phys Chem A 2013;117:13779–805.
[39] Rey M, Nikitin AV, Tyuterev VLG. First principles intensity calculations of the methane rovibrational spectra in the infrared up to 9300 cm^{-1}. Phys Chem Chem Phys 2013;15:10049–61.
[40] Rey M. Private communication.
[41] Nikitin AV, Mikhailenko S, Morino I, Yokota T, Kumazawa R, Watanabe T. Isotopic substitution shifts in methane and vibrational band assignment in the 5560–6200 cm^{-1} region. J Quant Spectrosc Radiat Transf 2009;110:964–73.
[42] Rey M, Nikitin AV, Tyuterev VLG. Predictions for methane spectra from potential energy and dipole moment surfaces: isotopic shifts and comparative study of $^{13}CH_4$ and $^{12}CH_4$. J Mol Spectrosc 2013;291:85–97.